1 **Title: An insula-central amygdala circuit for behavioral inhibition**

2

3 **Abbreviated title: A circuit for behavioral inhibition**

4

5 **Authors:** Hillary Schiff[1]§, Anna Lien Bouhuis[1,2], Kai Yu[1], Mario A. Penzo[1]§, Haohong
6 Li[1]§, Miao He[3], Bo Li[1,#]

7

8 **Affiliations:**
9 1. Cold Spring Harbor Laboratory, Cold Spring Harbor, NY11724, USA.
10 2. Swammerdam Institute for Life Sciences, Center for Neuroscience, University of
11    Amsterdam, 1098 XH, Amsterdam, the Netherlands.
12 3. Institutes of Brain Science, State Key Laboratory of Medical Neurobiology,
13    Collaborative Innovation Center for Brain Science, Fudan University, Shanghai
14    200032, China.

15

16 § Current address: Stony Brook University (H.S.), Unit on the Neurobiology of Affective
17 Memory, National Institute of Mental Health, Bethesda, MD 20892, USA (M.P.),
18 Huazhong University of Science and Technology, Wuhan 430074, China (H.L.).

19

20 **# Corresponding author:**
21 Bo Li, PhD
22 1 Bungtown Road
23 Cold Spring Harbor NY 11724
24 Email: bli@cshl.edu

25

26 **Number of pages:** 34

27 **Number of figures:** 6

28 **Number of words** for Abstract: 221; Introduction: 760; and Discussion: 730.

29 **Total number of words:** 9,105

30 **Conflict of Interest:** The authors declare no competing financial interests.

42    **Abstract**

43    Predicting which substances are suitable for consumption during foraging is critical for

44    animals to survive. While food-seeking behavior is extensively studied, the neural circuit

45    mechanisms underlying avoidance of potentially poisonous substances remain poorly

46    understood. Here we examined the role of the insular cortex (IC) to central amygdala

47    (CeA) circuit in the establishment of such avoidance behavior. Using anatomic tracing

48    approaches combined with optogenetics-assisted circuit mapping, we found that the

49    gustatory region of the IC sends direct excitatory projections to the lateral division of the

50    CeA (CeL), making monosynaptic excitatory connections with distinct populations of

51    CeL neurons. Specific inhibition of neurotransmitter release from the CeL-projecting IC

52    neurons prevented mice from acquiring the "no-go" response, while leaving the "go"

53    response largely unaffected in a tastant (sucrose/quinine)-reinforced "go/no-go" task.

54    Furthermore, selective activation of the IC-CeL pathway with optogenetics drove

55    unconditioned lick suppression in thirsty animals, induced aversive responses, and was

56    sufficient to instruct conditioned action suppression in response to a cue predicting the

57    optogenetic activation. These results indicate that activity in the IC-CeL circuit is

58    necessary for establishing anticipatory avoidance responses to an aversive tastant, and is

59    also sufficient to drive learning of such anticipatory avoidance. This function of the IC-

60    CeL circuit is likely important for guiding avoidance of substances with unpleasant tastes

61    during foraging in order to minimize the chance of being poisoned.

62

63    **Significance Statement**

2

64    The ability to predict which substances are suitable for consumption is critical for

65    survival. Here we found that activity in the insular cortex (IC) to central amygdala (CeA)

66    circuit is necessary for establishing avoidance responses to an unpleasant tastant, and is

67    also sufficient to drive learning of such avoidance responses. These results suggest that

68    the IC-CeA circuit is critical for behavioral inhibition in anticipation of potentially

69    poisonous substances during foraging.

70

71    **Introduction**

72    The ability to suppress actions that can lead to harmful consequences is critical for

73    survival. For example, animals, including humans, stop consummatory behavior when

74    encountering food or liquid with an unpleasant taste, which indicates the existence of a

75    potentially poisonous substance. Animals are also capable of learning to use

76    environmental cues (such as an odor, color, location or context) to predict unpleasant

77    properties (such as a bitter taste, toxicity) of a substance, and subsequently using these

78    predictive cues to guide avoidance of the substance during foraging. While food

79    approaching and reward seeking behaviors are extensively studied (Balleine, 2005, 2011;

80    Kelley, 2004), the neural circuit mechanisms that underlie innate and learned suppression

81    of actions that may lead to food poisoning, or aversive consequences in general, are

82    poorly understood.

83

84    The insular cortex (IC), including the gustatory cortex (GC), plays an important role in

85    processing taste and visceral information (Accolla and Carleton, 2008; Katz et al., 2001;

86    Samuelsen and Fontanini, 2017; Yamamoto et al., 1985). The IC is also engaged in

3

87      various learning tasks, especially when learning to associate a neutral tastant (also known

88      as a conditioned stimulus, CS) with an intrinsically aversive stimulus (also known as an

89      unconditioned stimulus, US), or to associate a non-gustatory CS with an appetitive or

90      aversive tastant US (Bermudez-Rattoni, 2004; Kusumoto-Yoshida et al., 2015; Vincis

91      and Fontanini, 2016; Yasoshima and Yamamoto, 1998). In one such task, a "go/no-go"

92      task in which auditory "go" and "no-go" CSs predict the delivery of sucrose and quinine,

93      respectively, specific CS-evoked responses develop in the IC as rats learn the predictive

94      value of each CS (Gardner and Fontanini, 2014). IC neurons also show CS-evoked

95      responses in a conditioned food-approaching task (Kusumoto-Yoshida et al., 2015).

96      These findings indicate that associative learning driven by gustatory reinforcement

97      induces plastic changes in the IC, and suggest that the IC may participate in guiding

98      approach or avoidance responses during feeding or foraging behaviors. Consistently,

99      pharmacological and optogenetic inhibition of the IC impairs conditioned food

100     approaching behavior (Kusumoto-Yoshida et al., 2015). Nevertheless, whether the IC is

101     also essential for avoidance of aversive tastes remains unknown.

102

103     The central nucleus of the amygdala (CeA), including its lateral division (CeL), is a

104     prominent downstream structure of the IC. As it is also a direct recipient of taste

105     information from the brainstem (Carter et al., 2013), the CeA is anatomically positioned

106     to process convergent taste information. Indeed, it has been shown that the CeA encodes

107     taste identification and palatability, responses that follow those in the IC (Sadacca et al.,

108     2012). These findings suggest that the CeA may process and use the information

109     originating from the IC to influence taste-motivated behaviors.

110

111    The CeL plays an important role in the learning and expression of defensive behaviors

112    (Ciocchi et al., 2010; Goosens and Maren, 2003; Li et al., 2013; Wilensky et al., 2006), as

113    well as in reward-related behaviors and feeding (Gallagher et al., 1990; Kentridge et al.,

114    1991; Kim et al., 2017; Robinson et al., 2014; Seo et al., 2016). For instance, previous

115    studies showed that the somatostatin-expressing (SOM$^+$) subpopulation of neurons in the

116    CeL is essential for the acquisition and expression of conditioned freezing and action

117    suppression (Fadok et al., 2017; Li et al., 2013; Yu et al., 2016). The protein kinase C-δ-

118    expressing (PKC-δ$^+$) CeL neurons, on the other hand, participate in conveying aversive

119    US information, drive avoidance response, and are sufficient to instruct aversive learning

120    (Yu et al., 2017). Furthermore, it has been shown that CeA neurons, including PKC-δ$^+$

121    CeL neurons, are critical for suppression of feeding behavior (Cai et al., 2014; Petrovich

122    et al., 2009). As the CeL is a major direct downstream target of the IC, these findings

123    point to the possibility that the IC controls learning or expression of taste-motivated

124    behavioral inhibition through the IC-CeL circuit.

125

126    To test this hypothesis, we used anatomical, electrophysiological, and circuit based

127    manipulation approaches. We found that an excitatory monosynaptic connection exists

128    between the posterior division of the IC and the CeL in mice, and that activation of the

129    IC-CeL pathway excites specific subtypes of neurons within the CeL. Notably, selective

130    inhibition of CeL-projecting IC neurons specifically impairs the conditioned inhibitory

131    response to a cue predicting an aversive tastant. Furthermore, activation of the IC-CeL

132    circuit with optogenetics produces a powerful suppression of ongoing licking behavior in

5

133 thirsty mice, induces avoidance behavior, and is sufficient to instruct conditioned lick

134 suppression. These results reveal an important role of the IC-CeL circuit in the

135 establishment of anticipatory behavioral inhibition, in particular the inhibition of

136 consummatory behavior in response to cues predicting an unpleasant taste.

137

138 **Materials and Methods**

139 **Animals**

140 Before surgery, mice were group-housed under a 12-h light-dark cycle (7 a.m. to 7 p.m.

141 light) with food and water freely available. The *Som-cre* (Taniguchi et al., 2011), *Ai14*

142 (Madisen et al., 2010), *Prkcd-cre* (Haubensak et al., 2010), and *Rosa26-stop^{flox}-tTA* (Li et

143 al., 2010) mice were described previously and were purchased from the Jackson

144 Laboratory. All mice were bred onto C57BL/6J genetic background. The *Som-cre;Ai14*

145 mice, which were heterozygous for both the Cre allele and the Lox-Stop-Lox-tdTomato

146 allele, were bred by crossing homozygous *Som-cre* mice with homozygous *Ai14* reporter

147 mice. Male mice of 40–80 d of age were used for behavioral and anatomical experiments.

148 Male and female mice of 35-45 d of age were used for *in vitro* slice physiology

149 experiments. Behavioral experiments were performed during the light cycle. All

150 procedures involving animals were approved by the Institute Animal Care and Use

151 Committees of Cold Spring Harbor Laboratory and carried out in accordance with US

152 National Institutes of Health standards.

153

154 **Viral vectors**

6

155 Most of the adeno-associated viruses (AAV) were produced by the University of North

156 Carolina vector core facility or the University of Pennsylvania vector core and have

157 previously been described (Ahrens et al., 2015; Penzo et al., 2015; Stephenson-Jones et

158 al., 2016; Yu et al., 2016): AAV9-Ef1a-DIO-eYFP, AAV9-Ef1a-DIO-hChR2(H134R)-

159 eYFP, AAV9-CAG-ChR2-GFP, AAV9.CAG.Flex.TeLC-eGFP.WPRE.bGH, and AAV-

160 TRE-hGFP-TVA-G. The AAV8.2-hEF1α-DIO-synaptophysin-mCherry was produced by

161 the MIT Viral Gene Transfer Core. The EnvA-pseudotyped, protein-G-deleted rabies-

162 EnvA-SAD-ΔG-mCherry virus was produced by the Viral Vector Core Facility at Salk

163 Institute (Penzo et al., 2015). CAV2-Cre was purchased from Montpellier vector platform

164 (Plateforme de Vectorologie de Montpellier (PVM), Biocampus Montpellier,

165 Montpellier, France) (Penzo et al., 2015; Stephenson-Jones et al., 2016). All viral vectors

166 were stored in aliquots at −80 °C until use.

167

168 **Histology**

169 Animals were deeply anesthetized and transcardially perfused with PBS, followed by

170 perfusion with 4% paraformaldehyde (PFA) in PBS. Brains were dissected out and

171 postfixed in 4% PFA at 4°C for three hours followed by cryoprotection in a PBS-buffered

172 sucrose (30%) solution until brains were saturated (~36 h). 50 μm coronal brain sections

173 were cut on a freezing microtome (SM 2010R, Leica). Brain sections were first washed in

174 PBS (3 x 5 min) at room temperature (RT) and then were blocked in 3% normal goat

175 serum (NGS) in PBST (0.3% Triton X-100) for 30 min at RT, followed by incubation

176 with primary antibodies overnight at 4 °C. Sections were then washed with PBS (4 x 15

177 min) and incubated with fluorescent secondary antibodies at RT for 2 hours. After

7

178    washing with PBS (4 x 15 min), sections were mounted onto glass slides with

179    Fluoromount-G (Beckman Coulter). Images were taken using a LSM 780 laser-scanning

180    confocal microscope (Carl Zeiss).

181

182    **Electrophysiology**

183    For electrophysiological experiments, mice were anesthetized with isoflurane,

184    decapitated and their brains quickly removed and chilled in ice-cold dissection buffer

185    (110.0 mM choline chloride, 25.0 mM $NaHCO_3$, 1.25 mM $NaH_2PO_4$, 2.5 mM KCl, 0.5

186    mM $CaCl_2$, 7.0 mM $MgCl_2$, 25.0 mM glucose, 11.6 mM ascorbic acid and 3.1mM

187    pyruvic acid, gassed with 95% $O_2$ and 5% $CO_2$). Coronal slices (300 μm) containing the

188    amygdala complex were cut in dissection buffer using a HM650 Vibrating-blade

189    Microtome (Thermo Fisher Scientific). Slices were immediately transferred to a storage

190    chamber containing artificial cerebrospinal fluid (ACSF) (118 mM NaCl, 2.5 mM KCl,

191    26.2 mM $NaHCO_3$, 1 mM $NaH_2PO_4$, 20 mM glucose, 2 mM $MgCl_2$ and 2 mM $CaCl_2$, at

192    34 °C, pH 7.4, gassed with 95% $O_2$ and 5% $CO_2$). After 40 min recovery time, slices

193    were transferred to RT (20–24°C) and perfused with ACSF constantly.

194

195    Simultaneous whole-cell patch-clamp recordings from pairs of $SOM^+$ and $SOM^-$ CeL

196    neurons were obtained with Multiclamp 700B amplifiers (Molecular Devices).

197    Recordings were under visual guidance using an Olympus BX51 microscope equipped

198    with both transmitted light illumination and epifluorescence illumination, and $SOM^+$ cells

199    were identified based on their fluorescence (tdTomato). To evoke IC-driven synaptic

200    transmission onto CeL neurons, the AAV-ChR2-YFP was injected into the IC of *Som-*

8

201    *Cre;Ai14* mice and allowed to express for 3 weeks. Acute brain slices were prepared, and

202    a blue light was used to stimulate ChR2-expressing axons in the CeL. The light source

203    was a single-wavelength LED system ($\lambda$ = 470 nm; CoolLED.com) connected to the

204    epifluorescence port of the Olympus BX51 microscope. 1 ms light pulses were triggered

205    by a TTL signal from the Clampex software to drive synaptic responses. Light pulses

206    were delivered every 10 seconds and synaptic responses were low-pass filtered at 1 KHz

207    and recorded at holding potentials of −70 mV (for AMPA-receptor-mediated responses)

208    and +40 mV (for NMDA-receptor-mediated responses). NMDA-receptor-mediated

209    responses were quantified as the mean current amplitude from 50-60 ms after stimulation.

210    Evoked EPSCs were recorded in ACSF with 100 µM picrotoxin to block inhibitory

211    synaptic transmission. The internal solution for voltage-clamp experiments contained 115

212    mM cesium methanesulphonate, 20 mM CsCl, 10 mM HEPES, 2.5 mM $MgCl_2$, 4 mM

213    $Na_2$-ATP, 0.4 mM $Na_3$GTP, 10 mM Na-phosphocreatine and 0.6 mM EGTA (pH 7.2).

214    To assess presynaptic function, a paired-pulse stimulation protocol (50 ms inter-stimulus

215    interval) was used to evoke double-EPSCs, and paired-pulse ratio (PPR) was quantified

216    as the ratio of the peak amplitude of the second EPSC to that of the first EPSC.

217

**Monosynaptic tracing with pseudotyped rabies virus**

219    Retrograde tracing of monosynaptic inputs onto genetically-defined cell populations of

220    CeL was performed and described in our previous study (Penzo et al., 2015), and the data

221    presented here were generated from the same study but were not published previously.

222    Briefly, the *Som-cre;Rosa26-stop$^{flox}$-tTA* mice and the *Prkcd-cre;Rosa26-stop$^{flox}$-tTA*

223    mice, which express tTA in $SOM^+$ cells and PKC-$\delta^+$ cells, respectively, were injected

9

224   into the CeL with the AAV-TRE-hGFP-TVA-G (0.2–0.3 μl) that expresses the following

225   components in a tTA-dependent manner: a fluorescent reporter histone GFP (hGFP);

226   TVA (which is a receptor for the avian virus envelope protein EnvA); and the rabies

227   envelope glycoprotein (G). Two weeks later the mice were injected in the same location

228   with the rabies-EnvA-SAD-ΔG-mCherry (1.2 μl), a rabies virus that is pseudotyped with

229   EnvA, lacks the envelope glycoprotein, and expresses mCherry. This method ensures that

230   the rabies virus exclusively infects cells expressing TVA. Furthermore, complementation

231   of the modified rabies virus with envelope glycoprotein in the TVA-expressing cells

232   allows the generation of infectious particles, which then can trans-synaptically infect

233   presynaptic neurons.

234

235   **Stereotaxic surgery**

236   Standard surgical procedures were followed for stereotaxic injection (Li et al., 2013;

237   Penzo et al., 2015). Briefly, mice were anesthetized with ketamine (100 mg per kg of

238   body weight) supplemented with dexmedetomidine hydrochloride (0.4 mg per kg) and

239   positioned in a stereotaxic injection frame (myNeuroLab.com). A digital mouse brain

240   atlas was linked to the injection frame to guide the identification and targeting (Angle

241   Two Stereotaxic System, myNeuroLab.com).

242

243   Viruses (~0.4 μl) were delivered with a glass micropipette (tip diameter, ~5 μm) through

244   a skull window (1–2 $mm^2$) by pressure applications (5–20 psi, 5–20 ms at 0.5 Hz)

245   controlled by a Picrospritzer III (General Valve) and a pulse generator (Agilent). The

246   injection was performed at the following stereotaxic coordinates for CeL: 1.18 mm

10

247 posterior, 2.9 mm lateral, and 4.6 mm ventral from bregma; and for IC: 0.10 mm

248 posterior, 3.90 mm lateral, and 4.20 mm ventral from bregma. For optogenetic

249 experiments, immediately after viral injection, an optical fiber (core diameter, 105 μm;

250 Thorlabs, Catalog number FG105UCA) was implanted 300 μm above the center of viral

251 injection. The optical fiber together with the ferrule (Thorlabs) was secured to the skull

252 with C&B-Metabond Quick adhesive luting cement (Parkell Prod), followed by dental

253 cement (Lang Dental Manufacturing).

254

255 Following the above procedures, a small piece of metal bar was mounted on the skull,

256 which was used to hold the mouse in the head fixation frame during behavior

257 experiments.

258

259 **Behavioral tasks**

260 *Licking Behavior*

261 Water deprivation started 23 hours before training. Mice were trained in the head fixation

262 frame for 10 minutes daily. A metal spout was placed in front of the animal's mouth for

263 water delivery. The spout also served as part of a custom "lickometer" circuit, which

264 registered a lick event each time a mouse completed the circuit by licking the spout while

265 standing on a metal floor. The lick events were recorded by a computer through custom

266 software written in LabView (National Instruments). Each lick triggered a single opening

267 of a water valve calibrated to deliver 0.3 μl water.

268

269    It took mice 4–7 days to achieve stable licking, the criterion for which was 10-minute

270    continuous licking with no interval between licking longer than 10 seconds. We used a

271    lick suppression index to quantify animals' degree of photostimulation-evoked

272    suppression of licking behavior: Lick suppression index = $(L_{PRE} - L_{CS}) / (L_{PRE} + L_{CS})$,

273    where $L_{PRE}$ is the number of licks in the 5 s period before CS onset, and $L_{CS}$ is the

274    number of licks in the 5 s CS period (Yu et al., 2016).

275

276    ***Go/no-go task***

277    Water deprivation started 23 hours before training, and mice were habituated to the head

278    fixation frame for 20 minutes on the first day of training with access to water through the

279    metal spout. On following days, animals underwent 2 training sessions each day, one in

280    the morning and the other in the afternoon. The 2 sessions were at least 4 hours apart,

281    with each consisting of 100 trials. For the subsequent 3-6 sessions, mice were exposed

282    only to the "go" cue (a 1-s, 5-kHz pure tone) followed by the delivery of 4.5 µl of water.

283    After mice successfully retrieved water on at least 80% of the trials, they moved to the

284    next training phase, in which they were required to lick the spout at least 1 time during

285    the go cue in order for the water to be released. This phase took an additional 3-6 sessions

286    until the animals reached the criteria of 80% correct responses. Following this phase,

287    animals received 1 training session consisting of the go cue paired with the delivery of

288    sucrose solution (100 mM) instead of water.

289

290    The next phase consisted of 10 sessions of go/no-go training. During this phase, 50

291    presentations of the go cue were delivered randomly intermixed with 50 presentations of

12

292     the "no-go" cue (a 1-s white noise), with the constraint that either cue could not appear

293     more than 5 times in a row, and that the first trial was always a go cue. Licking the spout

294     during the no-go cue resulted in the delivery of quinine solution (4.5 µl, 5 mM). The mice

295     were required to lick at least once the spout during the 1 s window of cue presentation in

296     order to receive the US. During all phases of the experiment, brief suction (500 ms in

297     duration) near the spout was applied 3.5 s after tone onset to remove any residual solution

298     from the previous trial.

299

300     For analysis, trials were sorted into go trials and no-go trials. A correct response during a

301     go trial ("hit") occurred when the mouse successfully licked the spout during the go cue

302     and subsequently received sucrose. A correct response during a no-go trial ("correct

303     reject") occurred when the mouse successfully omitted the lick response during the no-go

304     cue and thus avoided quinine. The overall performance over the entire session was

305     calculated as the total correct responses divided by the total trials: overall performance =

306     (hits + correct rejects) / (total trials).

307

308     For the optogenetics experiments we used a modified version of this go/no-go task, in

309     which licking during the go cue led to water delivery (4.5 µl), whereas licking during the

310     no-go cue resulted in water delivery (4.5 µl) accompanied by laser stimulation. The laser

311     was delivered coincidentally with water delivery (50 ms after CS offset) at 20- or 30-Hz

312     for 2.5 seconds (the duration that the water would be available if the animal licked during

313     the no-go cue presentation). Suction was applied to remove any unconsumed water.

314     Animals received 8 training sessions in the final phase of this task.

13

315

316     *Real time place aversion (RTPA)*

317     As previously described (Stephenson-Jones et al., 2016), one side of a custom chamber

318     (23 × 33 × 25 cm; made from plexiglass) was assigned as the stimulation zone,

319     counterbalanced among mice. Mice were placed individually in the middle of the

320     chamber at the onset of the experiment, the duration of which was 30 min. Laser

321     stimulation (5-ms pulses delivered at 20 or 30 Hz) was triggered when mice entered the

322     stimulation zone, and lasted until mice exited the stimulation zone. Mice were videotaped

323     with a CCD camera interfaced with the Ethovision software (Noldus Information

324     Technologies), which was used to control the laser stimulation and extract the behavioral

325     parameters (position, time, distance, and velocity).

326

327     *In vivo optogenetics*

328     For bilateral optogenetic stimulation in the CeL, a branched patch-cord (Doric Lenses,

329     Catalog number BFP(2)_105/125/900-0.22_1m_FC-2xZF1.25) for light delivery was

330     connected at one end to a laser source ($\lambda$ = 473 nm, OEM Laser Systems) and at the other

331     end, which was composed of two terminals, to two CeL-implanted optical fibers through

332     sleeves (Thorlabs). For photostimulation-induced lick suppression, the stimuli were 5-ms

333     30-Hz light pulses (or across a range of frequencies) delivered for 5 s. For

334     photostimulation during RTPA, 5-ms 20- or 30-Hz light pulses were delivered. Laser

335     intensity was 10 mW measured at the end of optical fiber.

336

14

337    **Statistics and data presentation**

338    All data are presented as mean ± s.e.m. All statistics are indicated where used. Data were

339    analyzed with GraphPad Prism. Behavioral tests were performed by an investigator with

340    knowledge of the identity of the experimental groups. All behavior experiments were

341    controlled by computer systems, and data were collected and analyzed in an automated

342    and unbiased way. Virus-injected animals in which the injection or optical fiber

343    implantation was misplaced were excluded.

344

345    **Results**

346    To investigate the function of the IC-CeL circuit, we began by characterizing how IC

347    neurons innervate the major CeL cell types. We first used a modified rabies virus system

348    to trace the monosynaptic inputs onto CeL neurons (Callaway and Luo, 2015; Penzo et

349    al., 2015). This approach revealed a monosynaptic projection from the IC to the CeL

350    (Fig. 1A, B). In particular, IC neurons innervate both of the two major populations of the

351    CeL, the SOM$^+$ neurons and PKC-$\delta^+$ neurons (Fig. 1A, B). Notably, the IC was the only

352    cortical region identified by this approach to send monosynaptic projections to the CeL.

353    The CeL-projecting IC neurons were preferentially localized in the posterior part of the

354    IC, which overlaps at least partially with the GC (Fig. 1B).

355

356    As the IC also sends projections to the BLA (Allen et al., 1991), we next determined

357    whether the same IC neurons project to both the CeL and the BLA. To this end we

358    injected the CeL and BLA with the retrograde tracer AlexaFluor-488- or 555-conjugated

359    cholera toxin (CTB-488 or CTB-555), respectively (Fig. 1C). We found that CTB

15

360  reliably labeled CeL-projecting IC neurons (Fig. 1D), with a distribution pattern similar

361  to that of CeL-projecting IC neurons labeled by the rabies virus (Fig. 1B). CTB also

362  labeled a prominent population of BLA-projecting IC neurons, the vast majority of which

363  has a distribution pattern distinct from that of CeL-projecting IC neurons (Fig. 1D). This

364  result demonstrates that CeL-projecting neurons and BLA-projecting neurons in the IC

365  are largely non-overlapping populations.

366

367  To selectively target the CeL-projecting IC neurons and visualize their axonal

368  projections, we injected the CeL with a retrograde canine adenovirus expressing Cre

369  recombinase (CAV2-Cre) (Bru et al., 2010), followed by injecting the IC with an adeno-

370  associated virus harboring a double-floxed inverted open reading frame (AAV-DIO) that

371  expresses, in a Cre-dependent manner, a presynaptic protein synaptophysin tagged with a

372  fluorescent protein mCherry (AAV-DIO-synaptophysin-mCherry) (Fig. 1E). This

373  strategy led to the labeling of IC neurons that sent dense axonal fibers to the CeL (Fig.

374  1F). Sparse labeling of axon fibers in the BLA can also be detected (Fig. 1F), which

375  likely was caused by spillover of the CAV2-Cre to the BLA and thus the labeling of

376  BLA-projecting IC neurons. Though the ipsilateral CeL had the densest projections, we

377  also observed mCherry$^+$ axon terminals in the contralateral CeL, consistent with results

378  from retrograde tracing with CTB (data not shown). Altogether, the anatomical tracing

379  results demonstrate that the IC sends robust projections to the CeL, and that the IC-CeL

380  and IC-BLA are distinct circuits.

381

16

382   To assess the synaptic connectivity between the IC and CeL, we used the *Som-cre;Ai14*

383   mice, in which SOM$^+$ cells can be identified by their red fluorescence, and injected the IC

384   of these mice with an AAV expressing the light-gated cation channel channelrodhopsin-2

385   (AAV-ChR2-YFP) that allows photostimulation of axonal projections (Zhang et al.,

386   2006) (Fig. 2A). Approximately 3 weeks after the AAV injection, we prepared from these

387   mice acute brain slices containing the CeL, in which we recorded synaptic transmission

388   onto simultaneously patched pairs of adjacent SOM$^+$ (red-fluorescent) and SOM$^-$ (non-

389   fluorescent) CeL neurons in response to optogenetic stimulation of the IC inputs. Brief

390   light pulses evoked fast excitatory synaptic transmission in nearly all the recorded CeL

391   neurons (Fig. 2B). Notably, the AMPA receptor-mediated component of synaptic

392   transmission onto SOM$^+$ neurons was significantly greater than that onto SOM$^-$ neurons

393   (Fig. 2B-C). The NMDA receptor-mediated synaptic transmission onto these two

394   neuronal populations was not different. In a subset of these pairs, we also examined

395   paired-pulse ratio (PPR; see Methods) and found no significant difference between the

396   two cell types (Fig. 2C). These results indicate that IC inputs can activate both SOM$^+$

397   neurons and SOM$^-$ neurons in the CeL, with the latter being mainly PKC-$\delta^+$ neurons (Li

398   et al., 2013).

399

400   We reasoned that the IC-CeL circuit could have a role in behavioral inhibition, because

401   SOM$^+$ CeL neurons are essential for the generation of passive defensive responses,

402   including freezing behavior and action suppression (Fadok et al., 2017; Li et al., 2013;

403   Penzo et al., 2015; Yu et al., 2016), while PKC-$\delta^+$ CeL neurons convey aversive US

404   information and are sufficient to instruct aversive learning (Yu et al., 2017). To test this

17

405    hypothesis, we set out to inhibit the CeL-projecting IC neurons in mice and subsequently

406    trained these mice in a go/no-go task that engages the IC. We first injected the CeL with

407    the CAV2-Cre (Fig. 3A), and then injected the IC in the same mice with an AAV

408    expressing the tetanus toxin light chain (TeLC), which blocks neurotransmitter release

409    (Murray et al., 2011), or GFP (as a control) in a Cre-dependent manner (AAV-DIO-

410    TeLC-GFP or AAV-DIO-GFP, respectively) (Fig. 3A). As described above (Fig. 1E, F),

411    this strategy led to selective targeting of the IC-CeL circuit (Fig. 3B, C).

412

413    Four to five weeks following viral injections, we began training these mice in the go/no-

414    go task (see Methods), in which an auditory stimulus (go cue) predicts the delivery of a

415    palatable liquid (sucrose), while a different auditory stimulus (no-go cue) predicts the

416    delivery of an unpleasant liquid (quinine) (Fig. 3D). Mice need to learn to produce an

417    instrumental response (lick) during the go cue to receive sucrose, and inhibit that

418    response during the no-go cue to avoid quinine (Fig. 4A). Learning in this task has

419    previously been shown to be paralleled by the development of cue-specific responses in

420    IC neurons (Gardner and Fontanini, 2014).

421

422    We found that bilateral inhibition of synaptic transmission from CeL-projecting IC

423    neurons with TeLC markedly affected animals' behavior in the no-go trials, but left that

424    in the go trials of this task largely unaffected (Fig. 4A, B). Specifically, in the go trials,

425    mice in both the GFP group and the TeLC group showed stimulus-evoked licking (Fig.

426    4A), leading to similar performance (Fig. 4B); although closer inspection of these

427    animals' behavioral patterns revealed that the TeLC mice did not allocate their licking to

18

428    the CS and US period as much as the GFP control mice, especially on the final training

429    session (Fig. 4A,B). By contrast, in the no-go trials, while the GFP mice gradually

430    learned to withhold licking in response to the no-go cue, and thus successfully avoid

431    quinine in most of the trials towards the end of the training sessions (Fig. 4A, B), the

432    TeLC mice showed no sign of learning and thus were markedly impaired in performance

433    even at the end of the training sessions (Fig. 4A, B). The overall performance of the GFP

434    mice also showed a learning effect, evidenced by a gradual increase in performance over

435    the first 8 training sessions followed by asymptotic performance (Fig. 4B). On the other

436    hand, the animals expressing TeLC showed no such improvement with continued training

437    (Fig. 4B).

438

439    The impairment in behavioral inhibition observed during the no-go trials (or decrease in

440    the "correct reject") in the TeLC mice could be caused by a general increase in

441    responding. If so, then the performance of these mice in the go trials (measured as the

442    percentage of trials in which the mice made a response; or the "hit" rate) would also

443    increase. However we observed no such increase; in fact, the TeLC group showed a mild

444    decrease in hit rate, in particular in late sessions (Fig. 4B). The TeLC mice also showed a

445    reduced lick rate in response to the go cue, and had lick rate similar to that of the GFP

446    mice following the delivery of sucrose (Fig. 4A, C, D), further arguing against a general

447    increase in responding in these mice. In contrast, these mice showed an increased lick

448    rate specifically to the no-go cue and during the inter-trial interval (ITI) (Fig. 4A, C, E),

449    consistent with the notion that they were impaired in action suppression. We noticed that

450    the TeLC mice had a tendency to show increased lick rate following quinine delivery

19

451  compared with the GFP mice (Fig. 4D), suggesting that inhibiting the IC-CeL pathway

452  may partially impair the processing of aversive taste information during this task.

453  Alternatively, or additionally, the observations that the TeLC mice showed impaired

454  performance (although mild) and reduced lick rate during the go cue (Fig. 4B,C), as well

455  as impaired performance and increased lick rate during the no-go cue and quinine

456  delivery (Fig. 4B-D) could be explained by an impairment in these mice in anticipation of

457  salient outcomes, a function that has been attributed to the CeA (Balleine and Killcross,

458  2006; Haney et al., 2010; Roesch et al., 2012).

459

460  We also tested a subset of these animals on their sensitivity to increasing concentrations

461  of quinine during a free-licking session (10 minute). Similar to the GFP control group,

462  the TeLC group showed decreased average licking rate during this period (reflecting a

463  reduction in the total volume consumed) with increasing concentrations of quinine (Fig.

464  4F). This result is consistent with previous findings that lesions of the GC in rats do not

465  affect the amount of either quinine or sucrose solutions consumed at varying

466  concentrations (Hashimoto and Spector, 2014), and indicates that inhibition of CeL-

467  projecting IC neurons does not abolish animals' basic ability to process quinine's sensory

468  and aversive properties, at least when there is little cognitive demand. Together, these

469  results indicate that the IC-CeL pathway is required for establishing the learned,

470  anticipatory behavioral inhibition to avoid an aversive tastant.

471

472  Our results suggest that the CeL-projecting IC neurons preferentially regulate the no-go

473  response, consistent with the critical role of the CeL in processing aversive information

474    and in the learning and expression of avoidance behaviors. We therefore tested whether

475    activation of the IC-CeL pathway is sufficient to drive aversive responses as well as

476    instruct learning of an avoidance behavior. For this purpose we delivered the ChR2 or

477    GFP (as a control) specifically into CeL-projecting IC neurons bilaterally, using the

478    retrograde and intersectional strategy based on the CAV2-Cre as described above (Fig.

479    5A), and subsequently bilaterally implanted optical fibers over the CeL (Fig. 5B, C).

480

481    Four to five weeks following surgery, these mice were water deprived and trained to

482    achieve stable licking to a water spout, during which we delivered pulses of blue light

483    into the CeL. Photostimulation in the CeL in which the axon terminals originating from

484    the IC expressed ChR2 elicited robust suppression of licking, an effect that was

485    dependent on the frequency of stimulation (Fig. 5D, E). Furthermore, such optogenetic

486    activation of the IC-CeL pathway induced place aversion in a real time place aversion

487    (RTPA) task (Fig. 5F). By contrast, photostimulation in the CeL in which IC axons

488    expressed GFP induced neither lick suppression nor place aversion (Fig. 5D-F). These

489    results suggest that activation of the IC-CeL circuit is aversive, and is sufficient to induce

490    action suppression and avoidance responses.

491

492    To test whether activation of the IC-CeL circuit can be substituted for an aversive tastant

493    to instruct avoidance learning, similar to learning of the no-go response in the go/no-go

494    task, we trained the same mice as those used in Fig. 5 in a modified go/no-go task, in

495    which licking during one cue led to water delivery alone (the "laser-off" trials), whereas

496    licking during another cue resulted in water delivery coinciding with bilateral

21

497    photostimulation in the CeL (the "laser-on" trials) (Fig. 6A; also see Methods). We found

498    that the mice in which the IC-CeL pathway expressed ChR2 – and thus could be activated

499    by the photostimulation – showed reduced responding to the cue in the laser-on trials

500    compared with in the laser-off trials (Fig. 6B, C). By contrast, the mice in which the IC-

501    CeL pathway expressed GFP showed similar cue-evoked responding in the laser-on or

502    laser-off trials (Fig. 6B, C). We also verified that the photostimulation did not cause

503    obvious motor effects in either the ChR2 mice or the GFP mice in an open field setting

504    (Fig. 6D).

505

506    Of note, although optogenetic activation of the IC-CeL pathway was less effective than

507    quinine reinforcement, we observed a pattern of responding in these mice qualitatively

508    similar to that of the control animals trained on the standard sucrose/quinine go/no-go

509    task (Fig. 4B), in which the mice showed low levels of responding to the no-go cue and

510    high levels of responding to the go cue. Together, these results indicate that activation of

511    the IC-CeL pathway is sufficient to instruct the learning of anticipatory action

512    suppression. This mechanism is likely engaged when learning to avoid an aversive

513    outcome, such as an unpleasant tastant.

514

515    **Discussion**

516    In this study we examined the role of the IC-CeL circuit in the establishment of

517    behavioral inhibition for avoiding an unpleasant tastant. Using retrograde anatomic

518    tracing approaches, including the modified rabies virus-assisted tracing, together with

519    ChR2-based circuit mapping, we found that the GC region of the IC sends direct

520 excitatory projections to the CeL, which make monosynaptic connections with both the

521 SOM$^+$ and SOM$^-$ CeL neurons, with the latter being mainly PKC-$\delta^+$ neurons (Li et al.,

522 2013; Penzo et al., 2014). Specific inhibition of the CeL-projecting IC neurons with

523 TeLC prevented mice from acquiring the no-go response, and only mildly affected the go

524 response in a tastant (sucrose/quinine)-reinforced go/no-go task. Furthermore, selective

525 activation of the IC-CeL pathway with optogenetics drove unconditioned lick suppression

526 in thirsty animals, induced avoidance behavior, and was sufficient to instruct conditioned

527 action suppression in response to the cue that predicts the optogenetic activation. These

528 results demonstrate that activity in the IC-CeL circuit is necessary for establishing

529 anticipatory avoidance responses to an unpleasant tastant, and is also sufficient to drive

530 learning of such anticipatory avoidance responses.

531

532 The IC has been shown to contain regions with selective responses to distinct tastants

533 (Chen et al., 2011). As measured in anesthetized animals, these "hotspots" occupy non-

534 overlapping regions within the GC. The region with preferential responses to bitter tastes

535 resides in the posterior part of the GC, which corresponds approximately to the area of IC

536 we identified that sends the strongest projections to the CeL (also see (Allen et al.,

537 1991)). These findings suggest that the IC may preferentially convey information about

538 bitter/aversive tastants to the CeL, which in turn drive behavioral inhibition. Interestingly,

539 although the IC has been shown to be required for identifying and discriminating between

540 tastants (Katz et al., 2001; Peng et al., 2015; Sammons et al., 2016), we did not observe

541 an effect on quinine sensitivity when we selectively silenced the IC-CeL pathway with

542 TeLC (Fig. 4F), suggesting that the ability for bitter tastant identification and that for

543    processing the basic reinforcing properties of bitter tastants are preserved in these mice,

544    at least when cognitive demand is low.

545

546    The CeA, including the CeL, receives aversive information of different modalities

547    directly from the brainstem parabrachial nucleus (PBN) (Carter et al., 2013; Han et al.,

548    2015; Norgren et al., 1989; Sato et al., 2015). Previous studies have shown that the CeA

549    responds to noxious stimuli, such as footshocks that induce somatic pain (Han et al.,

550    2015; Radulovic et al., 1998), colorectal distension that induces visceral pain (Myers and

551    Greenwood-Van Meerveld, 2012), and lithium chloride, which induces malaise and is the

552    most commonly used US for inducing conditioned taste aversion (Lamprecht and Dudai,

553    1995). The CeA has also been implicated in taste processing (Sadacca et al., 2012) and

554    feeding behaviors (Cai et al., 2014). Thus, the CeA is anatomically poised to process

555    convergent somatosensory, visceral, gustatory and aversive information and may be

556    recruited by multiple neural circuits for action suppression in a variety of tasks, in which

557    the goal is to avoid unwanted consequences.

558

559    More recent studies, including those of our own, indicate that the CeA contains

560    functionally heterogeneous neuronal populations. SOM$^+$ CeL neurons control passive

561    defensive responses, such as freezing and action suppression (Fadok et al., 2017; Li et al.,

562    2013; Penzo et al., 2014; Penzo et al., 2015; Yu et al., 2016), whereas PKC-$\delta^+$ CeL

563    neurons are involved in conveying aversive US information and instructing aversive

564    learning (Yu et al., 2017). The PKC-$\delta^+$ CeL neurons have also been linked to suppression

565    of feeding (Cai et al., 2014). As both of these CeL populations receive direct excitatory

24

566     inputs from the IC (Fig. 1), they may contribute to distinct aspects of the IC-CeL circuit

567     function described in the current study. An intriguing possibility is that the SOM$^+$

568     population induces action suppression when excited by IC inputs, while the PKC-$\delta^+$

569     population regulates learning and potentially aversion when activated by the same inputs.

570     Some of the functions mediated by CeL neurons, in particular those by PKC-$\delta^+$ neurons,

571     are consistent with the findings that the CeA plays a role in alerting or attentional

572     processes, and can explain our observations suggesting that the IC-CeL circuit may have

573     a more general function in behavior, i.e., it influences performance and actions during not

574     only the no-go trials, but also the go trials of the go/no-go task, although the impact on

575     the no-go trials is much stronger.

576

577     **Figures**

578     **Figure 1. The IC sends monosynaptic projections to the amygdala.** (**A**) A schematic

579     of the experimental approach (see Methods). (**B**) Representative images of the tracing

580     result for SOM$^+$ (left) and PKC-$\delta^+$ (right) CeL neurons. Top, retrogradely labeled neurons

581     in the IC. Bottom, starter neurons in the CeL are identified by their co-expression of

582     mCherry and histone GFP (cells in yellow). Data in A & B were replicated in 3 mice for

583     each group, and were from the same injections reported in (Penzo et al., 2015). (**C**) Top:

584     a schematic of the experimental approach. Bottom: a representative image of the injection

585     sites. (**D**) The distribution of the BLA-projecting (red) and the CeL-projecting (green)

586     neurons in the IC. AIC, agranular insular cortex; GIC, granular insular cortex; DIC,

587     disgranular insular cortex. Data in C & D were replicated in two mice. (**E**) A schematic

588     of the experimental approach. (**F**) Representative images showing the mCherry$^+$ axons

25

589   (top), which originated from the CeL-projecting IC neurons (bottom). In the insets are

590   enlarged images of the boxed areas in the right, which are located in the amygdala (top)

591   and the IC (bottom).

592

593   **Figure 2: Functional connectivity between IC neurons and CeL neurons.**

594   (**A**) A schematic of the experimental design. AAV-ChR2-YFP was injected into the IC of

595   a *SOM;Ai14 mouse* (left), and patch clamp recording was performed in acute slices

596   containing the amygdala (right). (**B**) Sample traces of EPSCs recorded from a SOM$^+$ and

597   a SOM$^-$ CeL neuron, which were recorded simultaneously. The EPSCs were evoked by

598   optogenetic stimulation of the IC axons terminating in the CeL, with the AMPA receptor-

599   mediated EPSCs being stimulated with two pulses (50 ms inter-pulse interval) protocol.

600   (**C**) Quantification of the EPSC amplitude evoked by the first pulse mediated by AMPA

601   receptors is shown in the left panel, NMDA receptors is shown in the middle, and the

602   paired-pulse ratio (PPR) of AMPA receptor-mediated EPSCs is shown on the right. T-

603   tests revealed that the AMPA receptor-mediated EPSC was larger in SOM$^+$ than SOM$^-$

604   CeL neurons (AMPA, t(18) = 3, \*$P$ = 0.0085, NMDA, t(18) = 0.7, $P$ = 0.47, n = 10 pairs,

605   *t* test; PPR, t(12) = 1.8, $P$ = 0.1, n = 7 pairs, *t* test). Data in C are presented as mean ±

606   s.e.m.

607

608   **Figure 3. Experimental design to test the role of the IC-CeL circuit in a go/no-go**

609   **task.** (**A**) A schematic of the experimental design to selectively inhibit the IC-CeL

610   circuit. (**B**) Representative images showing the cells in the IC infected with GFP (left

611   panels) and TeLC-GFP (right panels) virus. In the lower panel are enlarged images of the

26

612    boxed areas in the images in the upper panel. (**C**) Axon terminals expressing GFP (left)

613    or TeLC-GFP (right), which originated from CeL-projecting IC neurons. (**D**) A schematic

614    of the go/no-go task.

615

616    **Figure 4. The IC-CeL circuit is required for suppression of behavioral responding.**

617    (**A**) Population histogram of licking behavior during the first and final sessions of go/no-

618    go training. Licking behavior is represented separately according to go (top panels) or no-

619    go (bottom panels) trials for both GFP (blue; n = 9) and TeLC (red; n = 7) mice. Dashed

620    line denotes the time window of CS delivery. US was delivered 50 ms after CS offset.

621    Shaded regions represent s.e.m. (**B**) Quantification of performance (the percentage of

622    correct responding trials) on the go/no-go task. For the go trials, the TeLC animals

623    showed a mild reduction in performance compared to GFP animals (two-way repeated

624    measures (RM) ANOVA revealed a significant interaction, but no main effects: main

625    effect of session, $F_{(9,126)} = 1.4$; $P = 0.2$; main effect of virus treatment, $F_{(1,14)} = 2.4$; $P$

626    $= 0.1$; interaction, $F_{(9,126)} = 2.8$; $P < 0.01$; \*$P < 0.01$, Post hoc Sidak's multiple

627    comparisons test). For the no-go trials, the TeLC animals showed a marked reduction in

628    performance compared to GFP animals (two-way RM ANOVA revealed a main effect of

629    session ($F_{(9,126)} = 2.84$; $P = 0.005$), a main effect of virus treatment ($F_{(1,14)} = 17.56$; $P$

630    $< 0.001$), and a significant interaction ($F_{(9,126)} = 4.8$; $P < 0.001$); \*$P < 0.05$, Post hoc

631    Sidak's multiple comparisons test). For the overall performance, the TeLC animals

632    showed a reduction in performance compared to GFP animals (two-way RM ANOVA

633    revealed a main effect of session ($F_{(9,126)} = 2.41$; $P = 0.01$), a main effect of virus

634    treatment ($F_{(1,14)} = 24.28$; $P < 0.01$), and a significant interaction ($F_{(9,126)} = 9.8$; $P <$

635     0.01). *$P < 0.01$, Post hoc Sidak's multiple comparisons test). (**C**) TeLC animals showed

636     a mild reduction in licking in response to the go cue (two-way RM ANOVA revealed a

637     significant interaction, but no main effects (main effect of session, $F(9,126) = 1.9$; $P =$

638     0.06; main effect of virus treatment, $F(1,14) = 4.1$; $P = 0.06$; interaction, $F(9,126) = 3.5$;

639     $P < 0.001$; *$P < 0.05$, Post hoc Sidak's multiple comparisons test). TeLC animals showed

640     an increase in licking in response to the no-go cue (two-way RM ANOVA revealed a

641     main effect of session ($F(9,126) = 3.76$; $P < 0.001$), a main effect of virus treatment

642     ($F(1,14) = 15.8$; $P = 0.001$), and a significant interaction ($F(9,126) = 4.45$; $P < 0.001$; *$P$

643     $< 0.05$, Post hoc Sidak's multiple comparisons test). (**D**) TeLC inhibition of the IC-CeL

644     circuit did not affect US-evoked licking rate ($P > 0.05$, two-way RM ANOVA). (**E**)

645     TeLC inhibition of the IC-CeL circuit increased the inter-trial licking rate (two-way RM

646     ANOVA revealed a main effect of session ($F(9,126) = 4.13$; $P < 0.001$), a main effect of

647     virus treatment ($F(1,14) = 15.73$; $P = 0.001$), and a significant interaction ($F(9,126) =$

648     2.08; $P = 0.037$); *$P < 0.05$, Post hoc Sidak's multiple comparisons test). (**F**) Quinine

649     sensitivity test showing lick rate during a 10-minute free-licking session for various

650     concentrations of quinine followed by a final session of water. TeLC inhibition of the IC-

651     CeL circuit did not affect quinine sensitivity (two-way RM ANOVA main effect of

652     quinine concentration, $F(7,84) = 16.3$, $P < 0.0001$; main effect of virus, $F(1,12) = 0.78$, $P$

653     $= 0.4$; interaction, $F(7,84) = 0.24$, $P = 0.97$). All data are presented as mean ± s.e.m.

654

655     **Figure 5. Optogenetic activation of the IC-CeL circuit is sufficient to induce action**

656     **suppression and avoidance behavior.** (**A & B**) Schematics of the experimental design.

657     (**C**) Representative images showing the locations of optical fiber implantation and green

28

658    axon fibers in the CeL, which originated from CeL-projecting IC neurons expressing

659    ChR2-YFP (left) or GFP (right). (**D**) Raster plots showing licking behavior for a GFP

660    (left) and a ChR2 (right) animal. Blue bars and shaded areas indicate the time window of

661    laser stimulation. (**E**) Quantification of the effect of the photostimulation on licking

662    behavior (suppression index) at different stimulation frequencies ($F_{(4,14)}$ = 4.375, $P$ =

663    0.017; *$P$ = 0.024, **$P$ = 0.007; one-way ANOVA followed by Sidak's multiple

664    comparisons test; 5-20Hz, n = 3 mice; 30Hz, n = 6 mice). (**F**) In a real-time place

665    avoidance behavioral paradigm, the ChR2 animals avoided the stimulation side (two-way

666    RM ANOVA main effect of stimulation side, $F_{(2,16)}$ = 4.27; $P$ = 0.03; main effect of

667    virus treatment, $F_{(1,8)}$ = 1.53; $P$ = 0.25); interaction, $F_{(2,16)}$ = 6.94; $P$ = 0.007; **$P$ =

668    0.005, Post hoc Sidak's multiple comparisons test; GFP, n = 4 mice, ChR2, n = 6 mice).

669

670    **Figure 6. Optogenetic activation of the IC-CeL circuit is sufficient to instruct**

671    **avoidance learning.** (**A**) A schematic of the experimental design. (**B**) Animal behavior is

672    quantified as the percentage of trials that animals chose to lick during CS presentation

673    (chosen trials) (GFP animals: two-way RM ANOVA showed a main effect of session

674    ($F_{(5,30)}$ = 5.59; $P$ < 0.001, no main effect of trial type ($F_{(1,6)}$ = 2.07; $P$ = 0.2, and a

675    significant interaction ($F_{(5,30)}$ = 3.05; $P$ = 0.024; Post hoc Sidak's multiple comparisons

676    tests revealed a significant difference in session 1 ($P$ = 0.004, n = 4 mice). ChR2 mice:

677    two-way RM ANOVA showed a main effect of trial type ($F_{(1,8)}$ = 5.7; $P$ = 0.04), no

678    main effect of session ($F_{(7,56)}$ = 1.35; $P$ = 0.25) or interaction ($F_{(7,56)}$ = 0.71; $P$ = 0.66;

679    n = 5 mice). (**C**) Quantification of the chosen trials in the final training session (two-way

680    repeated measures ANOVA revealed a main effect of group (GFP vs. ChR2) ($F_{(1,7)}$ =

681    8.19; $P$ = 0.024), a main effect of trial type (laser-off vs. laser-on) (F(1,7) = 6.59; $P$ =

682    0.037), and a significant interaction (F(1,7) = 5.778; $P$ = 0.047); *$P$ = 0.015, Post hoc

683    Sidak's multiple comparisons test).  (**D**) In an open field, laser stimulation did not affect

684    movement of mice (GFP or ChR2 mice), measured as average movement velocity over

685    10 trials ($P$ > 0.05, two-way RM ANOVA).  All data are presented as mean ± s.e.m.

686
687    **References**
688

689    Accolla, R., and Carleton, A. (2008). Internal body state influences topographical
690    plasticity of sensory representations in the rat gustatory cortex. Proc Natl Acad Sci U S A
691    *105*, 4010-4015.

692    Ahrens, S., Jaramillo, S., Yu, K., Ghosh, S., Hwang, G.R., Paik, R., Lai, C., He, M.,
693    Huang, Z.J., and Li, B. (2015). ErbB4 regulation of a thalamic reticular nucleus circuit
694    for sensory selection. Nat Neurosci *18*, 104-111.

695    Allen, G.V., Saper, C.B., Hurley, K.M., and Cechetto, D.F. (1991). Organization of
696    visceral and limbic connections in the insular cortex of the rat. J Comp Neurol *311*, 1-16.

697    Balleine, B.W. (2005). Neural bases of food-seeking: affect, arousal and reward in
698    corticostriatolimbic circuits. Physiol Behav *86*, 717-730.

699    Balleine, B.W. (2011). Sensation, Incentive Learning, and the Motivational Control of
700    Goal-Directed Action. In Neurobiology of Sensation and Reward, J.A. Gottfried, ed.
701    (Boca Raton (FL)).

702    Balleine, B.W., and Killcross, S. (2006). Parallel incentive processing: an integrated view
703    of amygdala function. Trends in Neurosciences *29*, 272-279.

704    Bermudez-Rattoni, F. (2004). Molecular mechanisms of taste-recognition memory. Nat
705    Rev Neurosci *5*, 209-217.

706    Bru, T., Salinas, S., and Kremer, E.J. (2010). An update on canine adenovirus type 2 and
707    its vectors. Viruses *2*, 2134-2153.

708    Cai, H., Haubensak, W., Anthony, T.E., and Anderson, D.J. (2014). Central amygdala
709    PKC-delta(+) neurons mediate the influence of multiple anorexigenic signals. Nat
710    Neurosci *17*, 1240-1248.

711    Callaway, E.M., and Luo, L. (2015). Monosynaptic Circuit Tracing with Glycoprotein-
712    Deleted Rabies Viruses. J Neurosci *35*, 8979-8985.

713   Carter, M.E., Soden, M.E., Zweifel, L.S., and Palmiter, R.D. (2013). Genetic
714   identification of a neural circuit that suppresses appetite. Nature *503*, 111-114.

715   Chen, X., Gabitto, M., Peng, Y., Ryba, N.J., and Zuker, C.S. (2011). A gustotopic map of
716   taste qualities in the mammalian brain. Science *333*, 1262-1266.

717   Ciocchi, S., Herry, C., Grenier, F., Wolff, S.B., Letzkus, J.J., Vlachos, I., Ehrlich, I.,
718   Sprengel, R., Deisseroth, K., Stadler, M.B.*, et al.* (2010). Encoding of conditioned fear in
719   central amygdala inhibitory circuits. Nature *468*, 277-282.

720   Fadok, J.P., Krabbe, S., Markovic, M., Courtin, J., Xu, C., Massi, L., Botta, P., Bylund,
721   K., Muller, C., Kovacevic, A.*, et al.* (2017). A competitive inhibitory circuit for selection
722   of active and passive fear responses. Nature *542*, 96-100.

723   Gallagher, M., Graham, P.W., and Holland, P.C. (1990). The amygdala central nucleus
724   and appetitive Pavlovian conditioning: lesions impair one class of conditioned behavior. J
725   Neurosci *10*, 1906-1911.

726   Gardner, M.P., and Fontanini, A. (2014). Encoding and tracking of outcome-specific
727   expectancy in the gustatory cortex of alert rats. J Neurosci *34*, 13000-13017.

728   Goosens, K.A., and Maren, S. (2003). Pretraining NMDA receptor blockade in the
729   basolateral complex, but not the central nucleus, of the amygdala prevents savings of
730   conditional fear. Behav Neurosci *117*, 738-750.

731   Han, S., Soleiman, M.T., Soden, M.E., Zweifel, L.S., and Palmiter, R.D. (2015).
732   Elucidating an Affective Pain Circuit that Creates a Threat Memory. Cell *162*, 363-374.

733   Haney, R.Z., Calu, D.J., Takahashi, Y.K., Hughes, B.W., and Schoenbaum, G. (2010).
734   Inactivation of the central but not the basolateral nucleus of the amygdala disrupts
735   learning in response to overexpectation of reward. J Neurosci *30*, 2911-2917.

736   Hashimoto, K., and Spector, A.C. (2014). Extensive lesions in the gustatory cortex in the
737   rat do not disrupt the retention of a presurgically conditioned taste aversion and do not
738   impair unconditioned concentration-dependent licking of sucrose and quinine. Chem
739   Senses *39*, 57-71.

740   Haubensak, W., Kunwar, P.S., Cai, H., Ciocchi, S., Wall, N.R., Ponnusamy, R., Biag, J.,
741   Dong, H.-W., Deisseroth, K., Callaway, E.M.*, et al.* (2010). Genetic dissection of an
742   amygdala microcircuit that gates conditioned fear. Nature *468*, 270-276.

743   Katz, D.B., Simon, S.A., and Nicolelis, M.A. (2001). Dynamic and multimodal responses
744   of gustatory cortical neurons in awake rats. J Neurosci *21*, 4478-4489.

745   Kelley, A.E. (2004). Ventral striatal control of appetitive motivation: role in ingestive
746   behavior and reward-related learning. Neurosci Biobehav Rev *27*, 765-776.

747  Kentridge, R.W., Shaw, C., and Aggleton, J.P. (1991). Amygdaloid lesions and stimulus-
748  reward associations in the rat. Behav Brain Res *42*, 57-66.

749  Kim, J., Zhang, X., Muralidhar, S., LeBlanc, S.A., and Tonegawa, S. (2017). Basolateral
750  to Central Amygdala Neural Circuits for Appetitive Behaviors. Neuron *93*, 1464-1479
751  e1465.

752  Kusumoto-Yoshida, I., Liu, H., Chen, B.T., Fontanini, A., and Bonci, A. (2015). Central
753  role for the insular cortex in mediating conditioned responses to anticipatory cues. Proc
754  Natl Acad Sci U S A *112*, 1190-1195.

755  Lamprecht, R., and Dudai, Y. (1995). Differential modulation of brain immediate early
756  genes by intraperitoneal LiCl. Neuroreport *7*, 289-293.

757  Li, H., Penzo, M.A., Taniguchi, H., Kopec, C.D., Huang, Z.J., and Li, B. (2013).
758  Experience-dependent modification of a central amygdala fear circuit. Nature
759  Neuroscience *16*, 332-339.

760  Li, L., Tasic, B., Micheva, K.D., Ivanov, V.M., Spletter, M.L., Smith, S.J., and Luo, L.
761  (2010). Visualizing the distribution of synapses from individual neurons in the mouse
762  brain. PLoS One *5*, e11503.

763  Madisen, L., Zwingman, T.A., Sunkin, S.M., Oh, S.W., Zariwala, H.A., Gu, H., Ng, L.L.,
764  Palmiter, R.D., Hawrylycz, M.J., Jones, A.R.*, et al.* (2010). A robust and high-throughput
765  Cre reporting and characterization system for the whole mouse brain. Nature
766  Neuroscience *13*, 133-140.

767  Murray, A.J., Sauer, J.F., Riedel, G., McClure, C., Ansel, L., Cheyne, L., Bartos, M.,
768  Wisden, W., and Wulff, P. (2011). Parvalbumin-positive CA1 interneurons are required
769  for spatial working but not for reference memory. Nat Neurosci *14*, 297-299.

770  Myers, B., and Greenwood-Van Meerveld, B. (2012). Differential involvement of
771  amygdala corticosteroid receptors in visceral hyperalgesia following acute or repeated
772  stress. Am J Physiol Gastrointest Liver Physiol *302*, G260-266.

773  Norgren, R., Nishijo, H., and Travers, S.P. (1989). Taste responses from the entire
774  gustatory apparatus. Ann N Y Acad Sci *575*, 246-263; discussion 263-244.

775  Peng, Y., Gillis-Smith, S., Jin, H., Trankner, D., Ryba, N.J., and Zuker, C.S. (2015).
776  Sweet and bitter taste in the brain of awake behaving animals. Nature *527*, 512-515.

777  Penzo, M.A., Robert, V., and Li, B. (2014). Fear conditioning potentiates synaptic
778  transmission onto long-range projection neurons in the lateral subdivision of central
779  amygdala. The Journal of neuroscience : the official journal of the Society for
780  Neuroscience *34*, 2432-2437.

781   Penzo, M.A., Robert, V., Tucciarone, J., De Bundel, D., Wang, M., Van Aelst, L.,
782   Darvas, M., Parada, L.F., Palmiter, R.D., He, M., *et al.* (2015). The paraventricular
783   thalamus controls a central amygdala fear circuit. Nature *519*, 455-459.

784   Petrovich, G.D., Ross, C.A., Mody, P., Holland, P.C., and Gallagher, M. (2009). Central,
785   but not basolateral, amygdala is critical for control of feeding by aversive learned cues. J
786   Neurosci *29*, 15205-15212.

787   Radulovic, J., Kammermeier, J., and Spiess, J. (1998). Relationship between fos
788   production and classical fear conditioning: effects of novelty, latent inhibition, and
789   unconditioned stimulus preexposure. The Journal of neuroscience : the official journal of
790   the Society for Neuroscience *18*, 7452-7461.

791   Robinson, M.J., Warlow, S.M., and Berridge, K.C. (2014). Optogenetic excitation of
792   central amygdala amplifies and narrows incentive motivation to pursue one reward above
793   another. J Neurosci *34*, 16567-16580.

794   Roesch, M.R., Esber, G.R., Li, J., Daw, N.D., and Schoenbaum, G. (2012). Surprise!
795   Neural correlates of Pearce-Hall and Rescorla-Wagner coexist within the brain. Eur J
796   Neurosci *35*, 1190-1200.

797   Sadacca, B.F., Rothwax, J.T., and Katz, D.B. (2012). Sodium concentration coding gives
798   way to evaluative coding in cortex and amygdala. J Neurosci *32*, 9999-10011.

799   Sammons, J., Bass, C., Victor, J., and Di Lorenzo, P. (2016). Gustatory cortical input
800   onto the nucleus of the solitary tract refines neuronal firing patterns and enhances
801   learning in the awake rat. Society for Neuroscience; 2016; San Diego, CA, USA.

802   Samuelsen, C.L., and Fontanini, A. (2017). Processing of Intraoral Olfactory and
803   Gustatory Signals in the Gustatory Cortex of Awake Rats. J Neurosci *37*, 244-257.

804   Sato, M., Ito, M., Nagase, M., Sugimura, Y.K., Takahashi, Y., Watabe, A.M., and Kato,
805   F. (2015). The lateral parabrachial nucleus is actively involved in the acquisition of fear
806   memory in mice. Mol Brain *8*, 22.

807   Seo, D.O., Funderburk, S.C., Bhatti, D.L., Motard, L.E., Newbold, D., Girven, K.S.,
808   McCall, J.G., Krashes, M., Sparta, D.R., and Bruchas, M.R. (2016). A GABAergic
809   Projection from the Centromedial Nuclei of the Amygdala to Ventromedial Prefrontal
810   Cortex Modulates Reward Behavior. J Neurosci *36*, 10831-10842.

811   Stephenson-Jones, M., Yu, K., Ahrens, S., Tucciarone, J.M., van Huijstee, A.N., Mejia,
812   L.A., Penzo, M.A., Tai, L.H., Wilbrecht, L., and Li, B. (2016). A basal ganglia circuit for
813   evaluating action outcomes. Nature *539*, 289-293.

814   Taniguchi, H., He, M., Wu, P., Kim, S., Paik, R., Sugino, K., Kvitsiani, D., Fu, Y., Lu, J.,
815   Lin, Y., *et al.* (2011). A resource of Cre driver lines for genetic targeting of GABAergic
816   neurons in cerebral cortex. Neuron *71*, 995-1013.

817    Vincis, R., and Fontanini, A. (2016). Associative learning changes cross-modal
818    representations in the gustatory cortex. Elife *5*.

819    Wilensky, A.E., Schafe, G.E., Kristensen, M.P., and LeDoux, J.E. (2006). Rethinking the
820    fear circuit: the central nucleus of the amygdala is required for the acquisition,
821    consolidation, and expression of Pavlovian fear conditioning. The Journal of
822    neuroscience : the official journal of the Society for Neuroscience *26*, 12387-12396.

823    Yamamoto, T., Yuyama, N., Kato, T., and Kawamura, Y. (1985). Gustatory responses of
824    cortical neurons in rats. II. Information processing of taste quality. J Neurophysiol *53*,
825    1356-1369.

826    Yasoshima, Y., and Yamamoto, T. (1998). Short-term and long-term excitability changes
827    of the insular cortical neurons after the acquisition of taste aversion learning in behaving
828    rats. Neuroscience *84*, 1-5.

829    Yu, K., Ahrens, S., Zhang, X., Schiff, H., Ramakrishnan, C., Fenno, L., Deisseroth, K.,
830    Zhou, P., Paninski, L., and Li, B. (2017). The central amygdala controls learning in the
831    lateral amygdala. bioRxiv 126649; doi: https://doiorg/101101/126649.

832    Yu, K., Garcia da Silva, P., Albeanu, D.F., and Li, B. (2016). Central Amygdala
833    Somatostatin Neurons Gate Passive and Active Defensive Behaviors. J Neurosci *36*,
834    6488-6496.

835    Zhang, F., Wang, L.P., Boyden, E.S., and Deisseroth, K. (2006). Channelrhodopsin-2 and
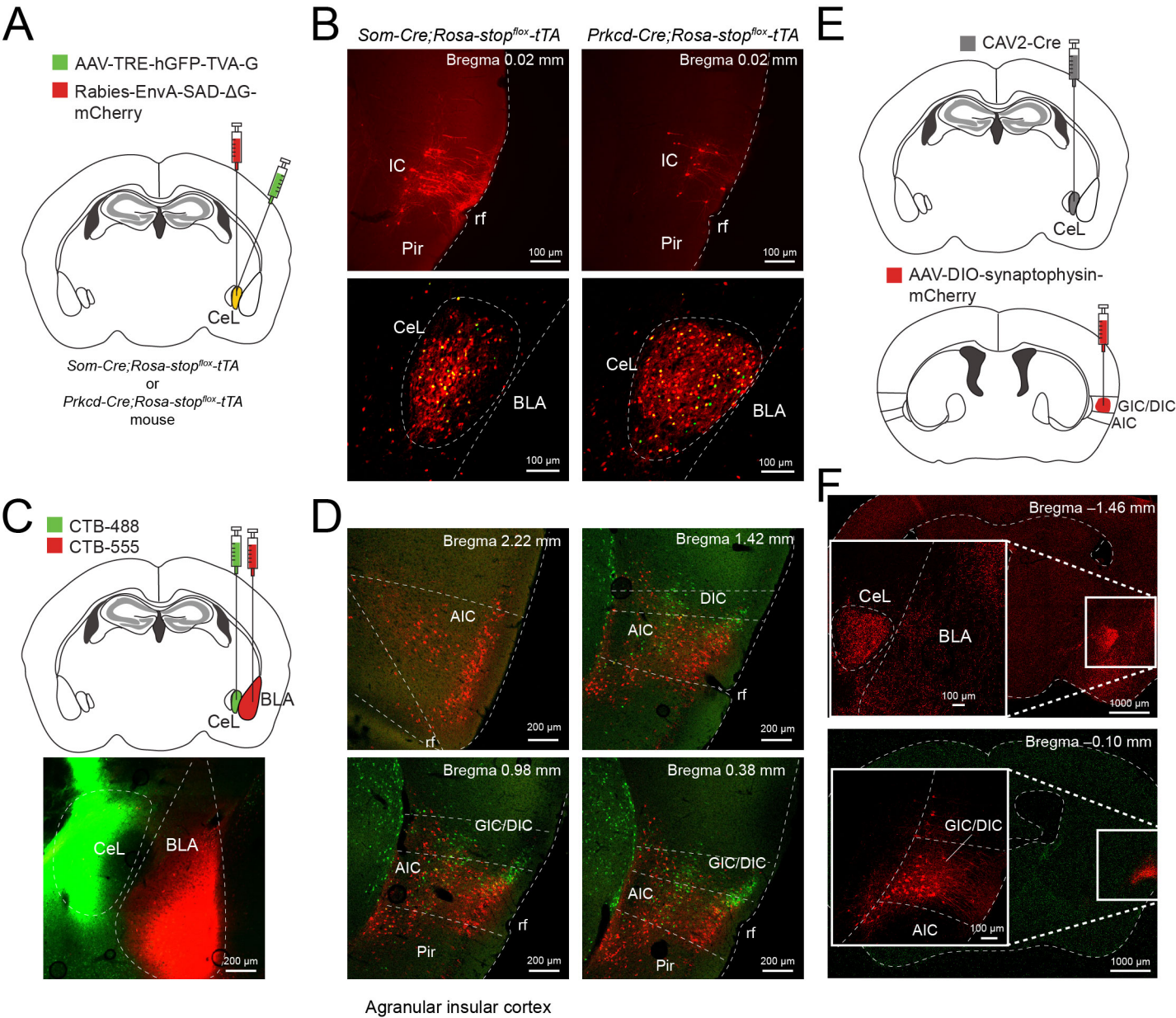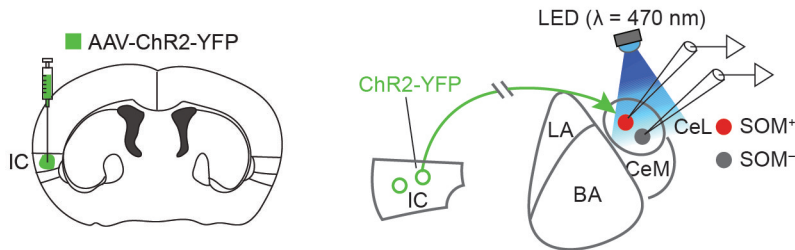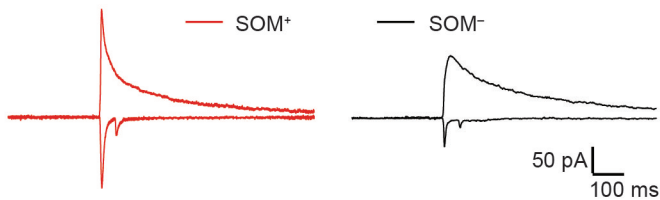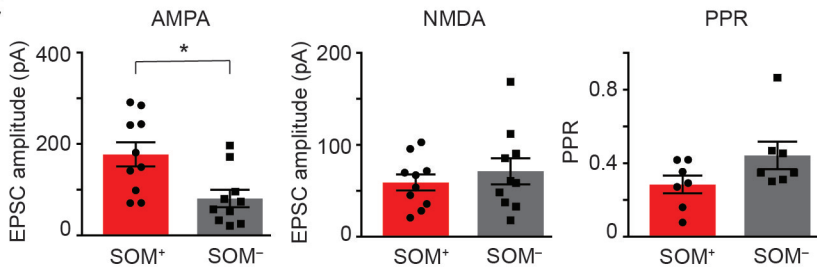836    optical control of excitable cells. Nat Methods *3*, 785-792.

837

**A**

AAV-TRE-hGFP-TVA-G

Rabies-EnvA-SAD-ΔG-mCherry

*Som-Cre;Rosa-stop^flox^-tTA*
or
*Prkcd-Cre;Rosa-stop^flox^-tTA*
mouse

CeL

**B**

*Som-Cre;Rosa-stop^flox^-tTA*    *Prkcd-Cre;Rosa-stop^flox^-tTA*

Bregma 0.02 mm    Bregma 0.02 mm

IC    IC
rf    rf
Pir    Pir
100 μm    100 μm

CeL    CeL
BLA    BLA
100 μm    100 μm

**C**

CTB-488
CTB-555

CeL    BLA

CeL    BLA
200 μm

**D**

Bregma 2.22 mm    Bregma 1.42 mm
AIC    DIC
      AIC
rf    rf
200 μm    200 μm

Bregma 0.98 mm    Bregma 0.38 mm
GIC/DIC    GIC/DIC
AIC    AIC
Pir    rf    Pir    rf
200 μm    200 μm

Agranular insular cortex

**E**

CAV2-Cre

CeL

AAV-DIO-synaptophysin-mCherry

GIC/DIC
AIC

**F**

Bregma −1.46 mm
CeL    BLA
100 μm    1000 μm

Bregma −0.10 mm
GIC/DIC
AIC
100 μm    1000 μm

Figure 1

**A**

AAV-ChR2-YFP

IC

ChR2-YFP

LED (λ = 470 nm)

LA

CeL

CeM

BA

IC

SOM⁺

SOM⁻

**B**

SOM⁺   SOM⁻

50 pA

100 ms

**C**

AMPA

*

EPSC amplitude (pA)

400

200

0

SOM⁺   SOM⁻

NMDA

EPSC amplitude (pA)

200

100

0

SOM⁺   SOM⁻

PPR

PPR

0.8

0.4

SOM⁺   SOM⁻

Figure 2

**A** CAV2-Cre | AAV-DIO-TeLC-GFP, or AAV-DIO-GFP

CeL | CeL

IC | IC

**B** GFP | TeLC-GFP

1000 μm | 1000 μm

IC | IC

IC | IC

100 μm | 100 μm

**C** CeL | CeL

BLA | BLA

200 μm | 200 μm

**D**

ITI = 10 ± 4 s

Go → Lick (sucrose)

Go → No lick (nothing)

No go → Lick (quinine)

No go → No lick (nothing)

Cue presentation and response window (1 s)

Figure 3

Figure 4

**A**

CAV2-Cre

AAV-DIO-ChR2-YFP, or
AAV-DIO-GFP

CeL    CeL    IC    IC

**B**

473-nm laser

Optical fiber

Speaker

head-fixation frame

water spout

CeL    LA

CeM    BA

**C**

ChR2-YFP

GFP

Fiber track    Fiber track

CeL    BLA    CeL    BLA

100 μm    100 μm

**E**

GFP

ChR2

Lick suppression index

30 Hz    5 Hz    10 Hz    20 Hz    30 Hz

*    **

**F**

GFP

ChR2

Time in left side (%)

100

Baseline    Left side stimu.    Right side stimu.

**

**D**

GFP

10

Trials

1

Light

−30    0    30
Time (s)

ChR2

10

Trials

1

Light

−30    0    30
Time (s)

Figure 5

Figure 6